Neutral-strange-particle production in p ^{20}Ne and pN interactions at 300 GeV

B. S. Yuldashev*
Department of Physics, University of Washington, Seattle, Washington 98195

S. M. Aliev, M. A. Alimov, K. K. Artykov, S. O. Edgorov, S. V. Inogamov, A. V. Khaneles, E. A. Kosonowski, S. L. Lutpullaev, N. Rasulov, T. P. Rodionova, K. T. Turdaliev, E. Turumov, and A. A. Yuldashev
The Physical Technical Institute, The Uzbek Academy of Sciences, Tashkent, 700084, U.S.S.R.

R. J. Loveless and D. D. Reeder
Department of Physics, University of Wisconsin, Madison, Wisconsin 53706
(Received 7 August 1990)

Data on multiplicity, correlations, and inclusive spectra of K_S^0 mesons and Λ^0 ($\bar{\Lambda}^0$) hyperons produced with $x_F \leq 0$ in inelastic p ^{20}Ne and pN interactions at 300 GeV are presented and compared. The inclusive cross sections for p ^{20}Ne (pN) with $x_F \leq 0$ are 61.1±2.8 mb (3.34±0.64 mb) for K_S^0, 40.8±2.5 mb (1.89±0.29 mb) for Λ^0, and 3.9±0.5 mb (0.31±0.08 mb) for $\bar{\Lambda}^0$. The multiplicity ratio for p ^{20}Ne and pN interactions is 1.58±0.16 for K_S^0, 1.95±0.23 for Λ^0, and 1.12±0.43 for $\bar{\Lambda}^0$. We have observed the $\Sigma^0(1193)$ hyperon and measured the average multiplicity ($n_{\Sigma^0}=0.049\pm0.027$) for $x_F \leq 0$. We have also observed the strange resonances $K^*(892)$, $K^*(1415)$, and $\Sigma^*(1385)$ with $x_F \leq 0$ and measured the fraction of V^0 coming from each resonance. Λ^0 polarization for $x_F \leq 0$ is measured and shows a decrease as $p_\perp$ increases [$p_\Lambda(p\,^{20}\text{Ne}) \approx -0.25$ at $p_\perp = 1.5$ GeV/c], in agreement with other experiments which measure polarization in the region $x_F \gg 0$. Since (43±7)% of the Λ^0 are produced in $\Sigma^0 \to \Lambda^0\gamma$ decays, the Λ^0 polarization is significantly greater than the measured values. Experimental results are compared to predictions of the Lund model and the dual parton model of soft hadron-nucleus and hadron-nucleon interactions.

I. INTRODUCTION

A study of strange-particle production by proton interactions with nuclei and nucleons can reveal important aspects of the dynamics of multiparticle production. According to modern models for a nonstrange initial state, the strange particles are produced from the sea of $s\bar{s}$ quarks.[1–3] Nuclear targets offer a unique opportunity since they serve as "analyzers" of the space-time evolution of hadronic (and/or quark-gluon) systems at very small distances.

Recent data obtained in interactions of protons with nuclei indicate surprisingly large cross sections for strange-particle production. Some authors interpret these results as a signal of non-nucleon degrees of freedom in a nucleus.[4–8]

Although a relatively large number of experiments measure the production of strange particles in hadron-nucleus (hA) interactions, most of them look at a limited kinematical region (e.g., see Refs. 9 and 10). At primary energies $E_0 \gtrsim 40$ GeV, only a few experiments have 4π-geometrical acceptance. This, in particular, leads to very little knowledge about the multiplicity of strange particles in hA interactions and, especially, about correlations between secondaries and strange hadrons, which can be due to strange resonance production.

In this paper we present first results on the inclusive production of K_S^0 and Λ^0 ($\bar{\Lambda}^0$) in incoherent p ^{20}Ne and inelastic pp (pn) interactions at 300 GeV for K_S^0 and Λ^0 with $x_F < 0$. We discuss results of measurements of production cross sections, multiplicities, and inclusive spectra as well as data on strange-resonance production and Λ^0 polarization.

To provide a context for understanding these data, we have shown comparisons to Monte Carlo calculations done in the framework of the Lund model[1,2] and the dual parton model, in a version proposed for soft hadron-nucleus and hadron-nucleon (hN) interactions.[3] We note that, in both the Lund model (LM) and the dual parton model (DPM), the Glauber theory is used to calculate the probability of ν successive collisions of the incoming projectile with the nucleons in the nucleus. The nucleon density in both modules is given by the Saxon-Woods potential. In the version of the Lund model we have used, the strange-quark suppression factor is 0.3. We emphasize that neither the formation lengths (or time) of secondary hadrons (which are made up of quarks) nor the rescattering of low-momentum secondaries found inside a nucleus (nuclear cascading) are taken into account in either model. In both the LM and DPM the quark combinatorics are used to calculate the probability of particles belonging to the known SU_3 multiplets.

II. EXPERIMENTAL PROCEDURE

The data are obtained from an exposure of the 30-in. Fermilab Ne-H_2 bubble chamber [(30.9±0.7)% molar Ne] to a 300-GeV/c diffractive proton beam. The results presented below were obtained from an analysis of approximately 26 000 pictures. The efficiency of double scanning was greater than 99% except for events with few charged tracks ($n_{ch} \leq 3$), for which the average efficiency was (87±3)%. All data were corrected for efficiency of double scanning (more details on scanning procedure can be found in Refs. 11 and 12).

All observed primary events are classified as "p Ne," "pp," and "pn," interactions in accordance with the standard procedure (e.g., see Ref. 13) for event separation in heavy-liquid bubble-chamber experiments. The total number of p ^{20}Ne interactions is determined on the basis of measured cross sections of p ^{20}Ne and pp interactions at 300 GeV.[13] We have excluded from the analysis both coherent p ^{20}Ne and elastic pp events. The secondary protons were identified by ionization and range in the momentum interval $0.12 \leq p \leq 1.2$ GeV/c. Of the negatively charged secondary hadrons, approximately 94% are π^- mesons. About 11% of positively charged relativistic (lightly ionizing) secondaries are fast ($p \geq 1.2$ GeV/c), unidentified protons.[13]

Secondary γ's were recorded by e^+e^- conversion and V^0 by the visible decays ($K_S^0 \to \pi^+\pi^-$, $\Lambda^0 \to p\pi^-$, $\bar{\Lambda}^0 \to \bar{p}\pi^+$) within the volume of the bubble chamber. The efficiency of finding of V^0 decays in double scanning was 98.6%. A separation of fast V^0 and γ was done after measurements and kinematical analysis (see below).

The data presented are based on measurements of 8153 primary events containing 5064 γ conversions and 825 V^0 decays in the chosen fiducial volume of bubble chamber. The total number of incoherent p ^{20}Ne events is $N(p\,^{20}\text{Ne}) = 5214$. The proton-nucleon ($pN$) events consist of pp interactions (on free hydrogen and quasifree protons of neon) and pn collisions (only on quasifree neutrons of neon) and their total number is $N(pN) = 3484$. Data for pN interactions are averaged over the target nucleon: $pN = 0.5(pp + pn)$.

In our analysis we regard the V^0 as unambiguously identified if the fit to only one hypotheses had $\chi^2 \leq 11$. We classified 59.3% of measured V^0 as unambiguous.

Ambiguous V^0 are resolved on the basis of two-body decay kinematics. The V^0-γ ambiguities are separated by the momentum component of the negative-decay particle transverse to the line of flight of the V^0 particle $p_\perp$. For γ's the $p_\perp$ distribution has a narrow peak at $p_\perp = 0$. A cut $p_\perp = 20$ MeV/c was used to separate V^0-γ ambiguities: $p_\perp \leq 20$ MeV/c for γ and $p_\perp > 20$ MeV/c for V^0. We estimate that only 0.8% of π^- mesons ($\bar{p}$) from $\Lambda^0(\bar{\Lambda}^0)$ decays and 0.2% of π^- from K_S^0 decays have $p_\perp$ less than 20 MeV/c. By applying this cut we identify 108 fast γ's in the V^0-γ sample.

The sample of V^0 which fit both the K_S^0/Λ^0 (or $K_S^0/\bar{\Lambda}^0$) hypothesis were also separated by $p_\perp$. All candidates having $p_\perp$ greater than 100 MeV/c were assumed to be K_S^0. A further separation of unresolved V^0 with $p_\perp < 110$ MeV/c was done statistically from an analysis of

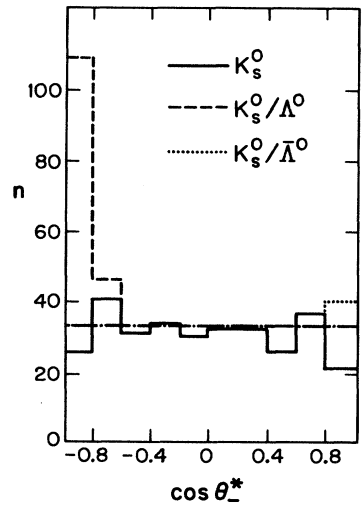

FIG. 1. The angular distribution of negatively charged decay particles in the rest system of the K_S^0 showing unambiguous K_S^0's (solid line), Λ^0/K^0 ambiguities (dashed line), and $\bar{\Lambda}/K^0$ ambiguities (dotted line). The dash-dotted line shows the expected flat distribution if all decays were K^0.

angular distributions (Fig. 1) of π^- mesons ($\bar{p}$) in the rest frame of K_S^0. From the requirement that the distribution for π^- mesons originating from K_S^0 decay is isotropic, we have determined that, among remaining V^0 ambiguities, 76.5% are Λ^0 hyperons, 5.8% are $\bar{\Lambda}^0$ hyperons, and 17.7% are K_S^0 mesons. The final sample of V^0 after assignment is shown in Table I.

In Fig. 2 we show $p_\perp$ distributions for π^- particles from the decay of K_S^0 and Λ^0 hyperons. These are consistent with the kinematics of two-body decay;

$$\frac{dN}{dp_\perp} \sim \frac{p_\perp}{p^*}(p^{*2} - p_\perp^2)^{-1/2}, \tag{1}$$

where p^* is the total momentum of decay particle in the rest system of the V^0 parent ($p^* = 101$ MeV/c for π^- or proton from Λ^0 decay and $p^* = 206$ MeV/c for K_S^0 decay).

TABLE I. Results of V^0 identification ($x_F \leq 0$).

Neutral-strange-particle decay	K_S^0	Λ^0	$\bar{\Lambda}^0$
Unambiguous V^0's	349	124	16
K_S^0/Λ^0	31.5	86.5	
$K_S^0/\bar{\Lambda}^0$	23.5		6.5
$K_S^0/\Lambda^0/\gamma$	3.3	14.7	
$K_S^0/\bar{\Lambda}^0/\gamma$	12.6		5.4
K^0/γ	16		
Λ^0/γ		20	
$\bar{\Lambda}^0/\gamma$			8
Total	435.9	245.2	35.9

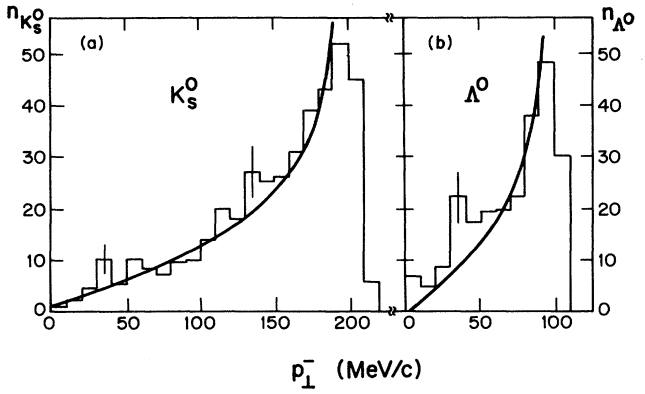

FIG. 2. The $p_\perp$ distributions for π^0 from decays of (a) K_S^0 and (b) Λ^0. The solid lines correspond to the expected distribution calculated from two-body kinematics.

For each V^0 decay, a geometrical efficiency weight was determined

$$W_g=\epsilon^{-1}=[1-\exp(-L_p/L)]^{-1}\ , \tag{2}$$

where ϵ is the geometrical efficiency of detecting a V^0, L_p is the length within a fiducial volume, $L=\beta\gamma c\tau_0$ is the decay length of the V^0 particle with Lorentz factor γ and velocity β, and τ_0 is the lifetime of a given V^0.

The average values of W_g are

$$\begin{aligned}&\langle W_g\rangle=1.39\pm0.08 \quad \text{for } K_S^0\ ,\\ &\langle W_g\rangle=1.60\pm0.10 \quad \text{for } \Lambda^0\ ,\\ &\langle W_g\rangle=2.11\pm0.22 \quad \text{for } \bar{\Lambda}^0\ .\end{aligned} \tag{3}$$

The loss of those events which occurred along the bubble-chamber line of sight was determined by correcting the distribution about the beam direction to isotropy $[k(\varphi)=1.09]$.

In order to correct the data for undetected V^0's, which decay at a small (≤ 2 cm) distance from the primary vertex or within the narrow cone of secondary charged particles, and interacted V^0's, we have compared the distribution in proper time τ of the V^0 decays to the expected distribution:

$$\frac{dN}{d\tau}=N_0[1-\exp(-\tau/\tau_0)]\ . \tag{4}$$

From this comparison we determined the average correction factors

$$\begin{aligned}&k(\tau_0)=1.14 \quad \text{for } K_S^0\\ &\text{and}\\ &k(\tau_0)=1.09 \quad \text{for } \Lambda^0(\bar{\Lambda}^0)\ .\end{aligned} \tag{5}$$

Finally, for each V^0, a weight is assigned

$$W(V^0)=W_g k(\varphi)k(\tau_0)B^{-1}\ , \tag{6}$$

where B is the branching ratio for the detectable V^0 decay mode:

$$B(K_S^0\to\pi^+\pi^-)=0.686$$

and

$$B(\Lambda^0\to p\pi^-)=B(\bar{\Lambda}^0\to\bar{p}\pi^+)=0.642\ .$$

The efficiency of detecting a fast V^0 is quite low largely due to the restricted volume of the bubble chamber. In order to avoid large statistical fluctuations and to minimize uncertainties due to corrections for these losses, we have restricted the following analysis to consider only V^0 emitted backward in the c.m. system (c.m.s.) of pp interactions, i.e., V^0 having the Feynman variable $x_F\leq 0$.

III. INCLUSIVE PRODUCTION CROSS SECTIONS

For the inclusive cross sections of K_S^0, Λ^0, and $\bar{\Lambda}^0$ production of $x_F\leq 0$ in pN interactions we have obtained

$$\begin{aligned}&\sigma(pN\to K_S^0X)_{x_F\leq 0}=3.34\pm0.64 \text{ mb/nucleon}\ ,\\ &\sigma(pN\to\Lambda^0X)_{x_F\leq 0}=1.89\pm0.29 \text{ mb/nucleon}\ ,\\ &\sigma(pN\to\bar{\Lambda}^0X)_{x_F\leq 0}=0.31\pm0.08 \text{ mb/nucleon}\ .\end{aligned} \tag{7}$$

The quoted errors include both statistical and systematic errors. These numbers are consistent with data for pp interactions at 303 GeV (Refs. 14 and 15) and at nearby energies.[16–19]

The corresponding inclusive cross sections for p ^{20}Ne interactions are found to be

$$\begin{aligned}&\sigma(p\,^{20}\text{Ne}\to K_S^0X)_{x_F\leq 0}=61.1\pm2.8 \text{ mb}\ ,\\ &\sigma(p\,^{20}\text{Ne}\to\Lambda^0X)_{x_F\leq 0}=40.8\pm2.5 \text{ mb}\ ,\\ &\sigma(p\,^{20}\text{Ne}\to\bar{\Lambda}^0X)_{x_F\leq 0}=3.9\pm0.5 \text{ mb}\ .\end{aligned} \tag{8}$$

If one assumes that inclusive cross section on a nuclear target of atomic number A is related to the cross section on a single nucleon at $x_F\leq 0$,

$$\sigma(pA\to V^0X)_{x_F\leq 0}=A^\alpha\sigma(pN\to V^0X)_{x_F\leq 0}\ . \tag{9}$$

Unfortunately, the A^α extrapolation works poorly for H_2, one of our two data points. It is necessary to correct the pN result using experimental measurements[20,21] showing that $\sigma_{\text{extrap}}(pN)=46$ mb compared to the measured $\sigma_{\text{meas}}(pN)=33$ mb. We then determine α from our p ^{20}Ne and corrected pN data:

$$\begin{aligned}&\alpha(K_S^0,x_F\leq 0)=0.86\pm0.06\ ,\\ &\alpha(\Lambda^0,x_F\leq 0)=0.91\pm0.05\ ,\\ &\alpha(\bar{\Lambda}^0,x_F\leq 0)=0.73\pm0.09\ ,\end{aligned} \tag{10}$$

where the systematic errors on the H_2 correction are not included.

These results are in reasonable agreement with the $K^\pm$ measurements[22–25] in the forward direction (e.g., $\alpha=0.92\pm0.03$ for K^+, 0.89 ± 0.03 for K^- at $y\sim 0$, and $p_\perp=1$ in Ref. 22). The data for K^0 and Λ^0 come from the forward region[26,20] and show a strong y dependence (~ 0.75 near $y\approx 1$ falling to 0.50 for $y\approx 3$ in Ref. 26). A

TABLE II. The average multiplicity of V^0 particles with $x_F \leq 0$ in p ^{20}Ne and pN interactions at 300 GeV. The experimental results are compared to calculations in the framework of the Lund model (Refs. 1 and 2) and the dual parton model (Ref. 3). The experimental errors include both statistical and systematic uncertainties, whereas the model calculations quote only statistical errors.

		$\langle n(K_S^0)\rangle$	$\langle n(\Lambda^0)\rangle$	$\langle n(\bar{\Lambda}^0)\rangle$
p ^{20}Ne	Experiment	0.172±0.008	0.115±0.007	0.0110±0.0012
	Lund model	0.232±0.005	0.154±0.004	0.0250±0.0002
	Dual parton model	0.174±0.003	0.121±0.003	0.0139±0.0010
pN	Experiment	0.109±0.010	0.059±0.006	0.0098±0.0036
	Lund model	0.123±0.003	0.080±0.002	0.0135±0.0010
	Dual parton model	0.113±0.003	0.075±0.002	0.0122±0.0010

reasonable extrapolation to $y \approx 0$ shows rough agreement with our data. We note, however, that it is difficult to compare data in limited kinematic regions with our data which is integrated over the backward hemisphere.

IV. AVERAGE MULTIPLICITY

The mean multiplicities of K_S^0, Λ^0, and $\bar{\Lambda}^0$ at $x_F \leq 0$ are given in Table II. In this table we also give the expected multiplicity according to calculations using the Lund model and the dual parton model. These model calculations were averaged over the nucleon target, as was done for pN interactions. The DPM agrees satisfactorily with p ^{20}Ne and pN data, while the Lund model overestimates (by about 30%) the average multiplicity of K_S^0, Λ^0, and $(\bar{\Lambda}^0)$ in both the p ^{20}Ne and pN interactions.

The ratios

$$R(V^0) = \frac{\langle n(V^0)\rangle_{p\,\mathrm{Ne}}}{\langle n(V^0)\rangle_{pN}} \tag{11}$$

of the average multiplicity of K^0, Λ^0, and $\bar{\Lambda}^0$ produced in the p ^{20}Ne and pN interactions at $x_F \leq 0$ are given in Table III, which shows both the experimental and model calculations (errors quoted for model calculations are statistical). It is interesting to note that the experimental value of $R(K_S^0)_{x_F \leq 0}$ coincides with the ratio of average multiplicity of γ conversions with $x_F \leq 0$ in p ^{20}Ne and pN interactions at 300 GeV:[12,27] $R(\gamma)_{x_F \leq 0} = 1.47 \pm 0.04$. Data from this exposure show that 98% of secondary γ conversions are produced in decays of π^0 and η^0 mesons.[27]

In p ^{20}Ne interactions at 300 GeV, the mean number $\langle \nu \rangle$ of target nucleons participating in an interaction is estimated to be $\langle \nu \rangle_{p\,\mathrm{Ne}} = 1.99$ in the optical approximation.[13,28–30] The ratio $R(\Lambda^0)$ for Λ^0 hyperons with $x_F \leq 0$ agrees with $\langle \nu \rangle_{p\,\mathrm{Ne}}$; this is not surprising because most Λ^0 at $x_F \leq 0$ are produced through fragmentation of target ("wounded") nucleons. From the data in Table III, the Lund model predicts larger values of $R(K_S^0)$ and $R(\bar{\Lambda}^0)$, although it agrees with experiment for $R(\Lambda^0)$, whereas the dual parton model prediction is consistent with the data in each case.

V. CORRELATION BETWEEN V^0 MULTIPLICITY AND CHARGED HADRONS

In Figs. 3(a) and 3(c) we show the average multiplicity of K_S^0 and Λ^0 with $x_F \leq 0$ as a function of the number n_- of negatively charged secondaries (approximately 94% of them are π^- mesons) in the p ^{20}Ne and pN interactions. For comparison, in Figs. 3(b) and 3(d) we also show data for pp interactions obtained in a hydrogen bubble-chamber experiment at 303 GeV.[14] Within errors, both experiments are in agreement.

The curves in Fig. 3 are predictions of the LM (dashed line) and the DPM (solid line). In p ^{20}Ne interactions neither of these models describe the data satisfactorily for $n_- \gtrsim 12$. However, events with $n_- \geq 12$ contribute less than 7% to the total inelastic cross section of p ^{20}Ne in-

TABLE III. The ratios of the average multiplicity for V^0 particles produced in p ^{20}Ne to that in pN interactions compared to the expected value as calculated by the Lund model and the dual parton model.

Particle	K_S^0	Λ^0	$\bar{\Lambda}^0$
Experiment	1.58±0.16	1.95±0.23	1.12±0.43
Lund model (Refs. 1 and 2)	1.87±0.06	1.93±0.07	1.85±0.14
Dual parton model (Ref. 3)	1.54±0.05	1.61±0.06	1.14±0.12

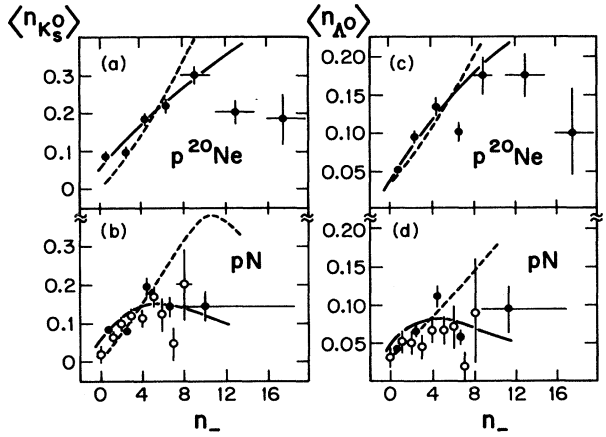

FIG. 3. The average multiplicity of K_S^0 [(a) and (b)] and Λ^0 [(c) and (d)] with $x_F \leq 0$ as a function of the number of negative hadrons in p ^{20}Ne [(a) and (c)] and pN [(b) and (d)] interactions. The open circles in (b) and (d) show the corresponding data for pp interactions at 303 GeV/c (Ref. 14). The curves correspond to the calculate predictions of the Lund model (dashed line) and the dual parton model (solid line).

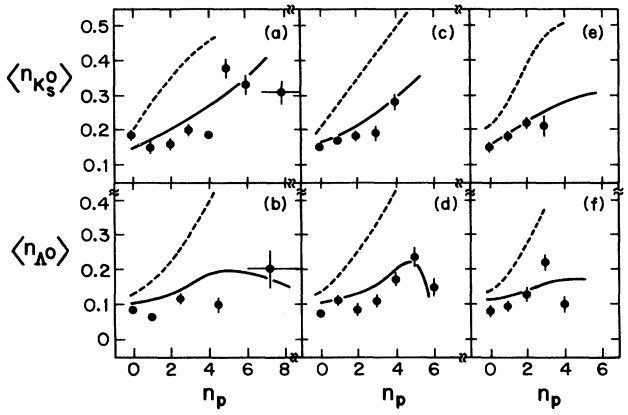

FIG. 4. The mean multiplicity of K_S^0 [(a), (c), and (e)] and Λ^0 [(b), (d), and (f)] with $x_F \leq 0$ as a function of the number of protons with momenta of $0.12 \leq p \leq 1.2$ GeV/c [(a) and (b)], $0.25 \leq p \leq 1.2$ GeV/c [(c) and (d)], $0.50 \leq p \leq 1.2$ GeV/c [(e) and (f)]. The curves show predictions of the LM (dashed curve) and the DPM (solid curve).

teractions at 300 GeV.[13] For pN reactions the predictions of the DPM are in better agreement with the data than the Lund model [Figs. 3(b) and 3(d)].

In the framework of some models of hA interactions (e.g., see Refs. 13 and 28–31) the multiplicity n_p of secondary protons (which are supposed to originate from the fragmentation of the nucleus) can be correlated with the average number of intranuclear collisions. Therefore, it is interesting to look for correlations between the number of secondary nucleons and the multiplicity of produced hadrons, such as V^0 particles.

In Figs. 4(a) and 4(b) we show average multiplicities of K^0 and Λ^0 with $x_F \leq 0$ as a function of the number n_p of identified protons with momenta of $0.12 \leq p \leq 1.2$ GeV/c in p ^{20}Ne interactions. It is seen that both $\langle n(K_S^0)\rangle_{x_F \leq 0}$ and $\langle n(\Lambda^0)\rangle_{x_F \leq 0}$ are increasing with n_p. A similar effect was observed for pions (charged and neutral)[12,13,27] and fast ($p_n \geq 1$ GeV/c) neutrons.[32] The observed increase of the mean number of produced hadrons with n_p can be, in principle, considered as an indication of a contribution from rescattering processes.

Data presented in Figs. 4(a) and 4(b) show that the Lund model calculations do not agree with our data. The dual parton model is in better agreement with the data, although the quantitative agreement is not outstanding. However, it should be emphasized that in both models the secondary nucleons are assumed to be knocked-out particles from a nucleus and no rescattering of either secondary pions or even relatively slow-recoil nucleons in a nucleus is taken into account.

As we have shown in Ref. 33, in p ^{20}Ne interactions at 300 GeV there are at least three categories of protons which are produced with momenta of $0.12 \leq p \leq 1.2$ GeV/c: (1) "evaporation" protons produced in the deexcitation of the nucleus or its heavy remnants, (2) protons produced in low-energy reactions in the nucleus,[34] and (3) knock-out protons from initial interaction or rescattering within the nucleus. The contribution of the latter to the total momentum spectrum of protons becomes dominant at $p \gtrsim 0.5$ GeV/c, while that of the "evaporation" protons determines the spectrum for $p \lesssim 0.2$ GeV/c. The second group of protons is revealed in the momentum interval $0.2 \lesssim p \lesssim 0.5$ GeV/c.

As an example, in Fig. 5 we compare the experimental spectrum of secondary protons in p ^{20}Ne interactions at 300 GeV (Ref. 33) with model calculations. The main disagreement between experiment and models is observed for protons with momenta $p \lesssim 0.5$ GeV/c, i.e., in the momentum region in which the protons are produced by processes ignored in the models. One can see from Figs.

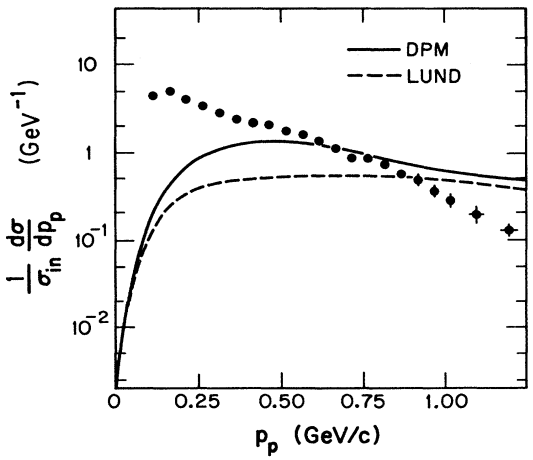

FIG. 5. The momentum distribution of secondary identified protons in p ^{20}Ne interactions. The curves correspond to the predictions of the LM (dashed line) and the DPM (solid line).

4(c) and 4(d) and 4(e) and 4(f) that the DPM predictions more closely describe the data as the momentum of secondary protons increased, but the LM is still in disagreement. For proton momenta above 1 GeV/c, both models overestimate the experimental spectrum.

VI. PRODUCTION OF Σ^0 HYPERONS

The relatively high detection efficiency for γ conversion ($\simeq 15\%$) in the H_2-neon bubble chamber[12,27] allows us to search for Σ^0 production through the observation of its decay $\Sigma^0 \rightarrow \Lambda^0\gamma$. In Fig. 6 we show the effective-mass distribution of the $(\Lambda^0\gamma)$ system for events in which at least one Λ^0 and one γ conversion were recorded. Data in Fig. 6 come from p ^{20}Ne interactions in which the $(\Lambda^0\gamma)$ system has $x_F \leq 0$. This plot has 287 mass combinations with 43 in the highest bin.

In the $M(\Lambda^0\gamma)$ spectrum there is a peak at the mass of the Σ^0 hyperon ($m_{\Sigma^0}=1.193$ GeV). The solid line is a fit of the experimental data to the sum of a Gaussian distribution [with dispersion determined by experimental resolution in mass of the $(\Lambda^0\gamma)$ system] and a polynomial background. The dashed curve represents the polynomial background fit obtained by random mixing of Λ^0 and γ from different events with the same kinematic constraints as the data. The resultant distribution is normalized to experimental area at $M(\Lambda^0\gamma) \geq 1.29$ GeV. The average multiplicity of Σ^0 hyperons produced at $x_F \leq 0$ in p ^{20}Ne interactions is

$$\langle n(\Sigma^0_{x_F \leq 0})\rangle_{p\,\mathrm{Ne}} = 0.049 \pm 0.027 \ . \tag{12}$$

From the data in Table II we calculate the fraction of Λ^0 produced via $\Sigma^0 \rightarrow \Lambda^0\gamma$ decays to be

$$f_{p\,\mathrm{Ne}}(\Lambda^0)_{x_F \leq 0} = \frac{\langle n(\Sigma^0_{x_F \leq 0})\rangle}{\langle n(\Lambda^0_{x_F \leq 0})\rangle} = 0.43 \pm 0.24 \ . \tag{13}$$

The corresponding ratio for our pN data is

$$f_{pN}(\Lambda^0)_{x_F \leq 0} = 0.34 \pm 0.16 \ .$$

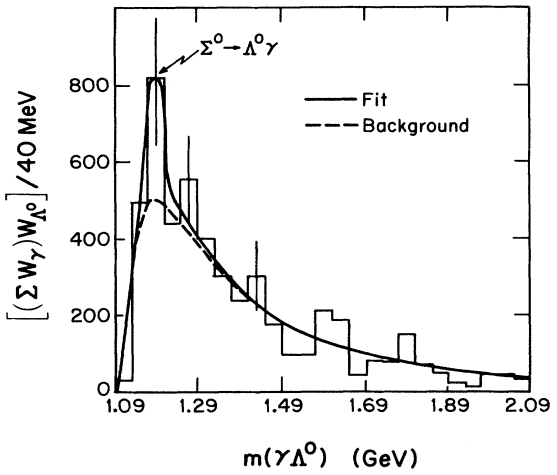

FIG. 6. The $(\Lambda^0\gamma)$ effective-mass distribution in p ^{20}Ne interactions. The dashed line is the random background; the solid line shows the fit for background plus Σ^0.

VII. PRODUCTION OF STRANGE RESONANCES

To search for production of strange resonances we used measurements of γ conversion[12,27] where we have observed narrow peak from a π^0 meson in the effective-mass distribution of $(\gamma\gamma)$ pairs. We selected events containing at least one recorded V^0 and two γ conversions from the π^0 region [$90 \leq M(\gamma\gamma) \leq 180$ MeV]. Because of limited statistics in this analysis, we present results obtained using the entire sample of $p(NeH_2)$ interactions, in which $(67.5 \pm 1.8)\%$ of events involve neon nuclei.[13]

A. $K^{*0}(892)$ and $K^{*0}(1415)$ production

In Fig. 7 the effective-mass distribution of the $K^0_S\pi^0$ system is presented for events in which the K^0_S has $x_F \leq 0$. This plot has 128 combinations with 24 in the highest bin. There are enhancements at $K^{*0}(892)$ and $K^{*0}(1415)$. The solid line represents a fit of the data to a sum of two Breit-Wigner functions and a polynomial background. The masses and widths of $K^{*0}(892)$ and $K^{*0}(1415)$ were fixed in the fit. The background distribution obtained from the fit is shown in Fig. 7 as a dashed line.

From this fit we determine that $(8.7 \pm 7.5)\%$ of K^0_S mesons with $x_F \leq 0$ are produced via decays of the $K^{*0}(892)$ resonance [$K^{*0}(892) \rightarrow K^0_S\pi^0$], and possibly $(3.1 \pm 5.6)\%$ via decays of the $K^{0*}_1(1440)$ resonance [$K^{0*}_1(1440) \rightarrow K^0_S\pi^0$]. These numbers are consistent with data from other experiments[15,35,36] at similar energies.

B. $\Sigma^0(1385)$ and $\Sigma^0(1670)$ production

We have also looked for production of $\Sigma^0(1385)$ and $\Sigma^0(1670)$ baryon resonances which have strangeness $s=-1$. These resonances can decay into $\Lambda^0\pi^0$ final states.[37]

In Fig. 8 we show the effective-mass distribution of the $(\Lambda^0\pi^0)$ system in which the Λ^0 have $x_F \leq 0$. This plot has 47 mass combinations with 10 in the highest peak. At masses corresponding to $\Sigma^0(1385)$ and maybe $\Sigma^0(1670)$

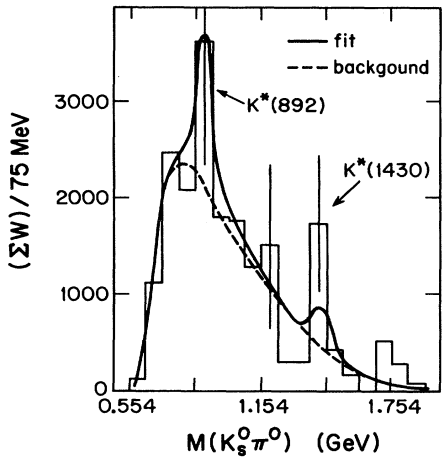

FIG. 7. The effective-mass distribution of the $(K_S^0\pi^0)$ system. The solid line represents the fit to background plus $K^{*0}(892)$ and $K_1^{*0}(1430)$; the dashed line shows the randomly generated background.

there are enhancements which can be attributed to the production of these resonances. The experimental data was fit to a sum of two Breit-Wigner functions (shown by the solid line) and a polynomial background (shown by the dashed curve). The masses and widths of these resonances were fixed and from the fit we determine that $(7.8\pm4.3)\%$ of Λ^0 with $x_F \leq 0$ are produced from $\Sigma^0(1385)\rightarrow\Lambda^0\pi^0$ decays. This result for $\Sigma^0(1385)$ production is consistent with other experiments.[15]

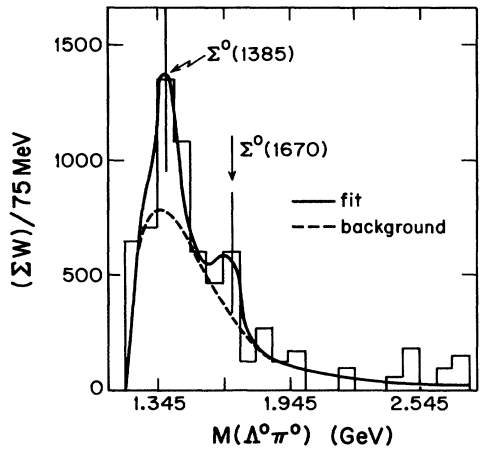

FIG. 8. The effective-mass spectrum of the $(\Lambda^0\pi^0)$ system. The solid line represents a fit to the background plus $\Sigma^0(1385)$ and $\Sigma^0(1670)$; the dashed line shows the randomly generated background.

VIII. INCLUSIVE SPECTRA

We also present data on the inclusive spectra of K_S^0 mesons and Λ^0 hyperons in p ^{20}Ne and pN interactions. In the study of hadron-nucleus interactions the region $x_F \leq 0$ is interesting because rescattering effects (cascading, etc.) reveal themselves in inclusive spectra of particles produced backward in the c.m.s. of hadron-nucleus collisions.

A. K_S^0 mesons

In Figs. 9(a) and 9(b) and 10(a) and 10(b) we show the c.m.s. (hadron-nucleus) rapidity, y^*, and the Feynman x_F distributions for K_S^0 mesons in p ^{20}Ne and pN interactions. For comparison, in Fig. 9(b) we also show data for pp interactions at 303 GeV/c;[14] there is a good agreement between the two experiments. The curves in Figs. 9 and 10 correspond to the expected distributions as calculated by the Lund model (dashed lines) and the dual parton model (solid lines) for p ^{20}Ne and pN interactions, respectively. The models are in rough agreement with the data, although the Lund model overestimates the K_S^0 multiplicity in the central region for p ^{20}Ne interactions

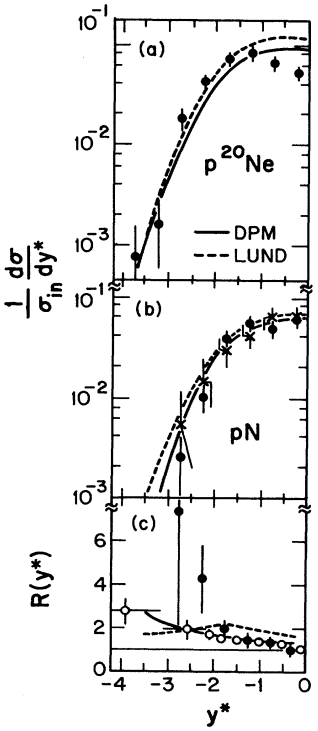

FIG. 9. The rapidity y^* in the center-of-mass system for K_S^0 in the (a) p ^{20}Ne and (b) pN interactions. Also shown in (b) are data for pp interactions at 303 GeV/c (Ref. 14) (crosses). In (c) the ratio of the normalized rapidity spectra $R(y^*)$ for p ^{20}Ne and pN interactions [see Eq. (14) in the text] is shown for K_S^0 (solid circles) and γ conversions (Refs. 12 and 28) (open circles). The curves are the predictions of the LM (dashed) and the DPM (solid) for K_S^0.

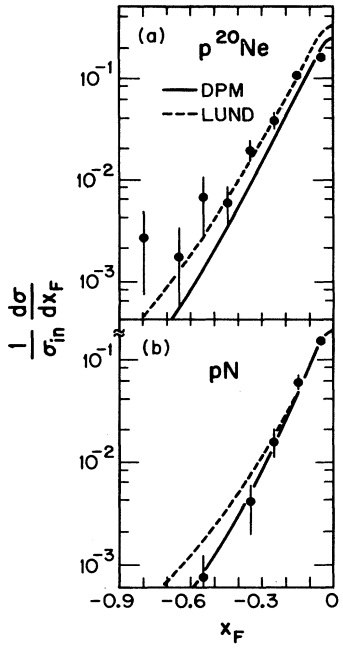

FIG. 10. The Feynman variable x_F for K_S^0 in the p ^{20}Ne and pN interactions. The curves show the predictions of the LM (dashed) and the DPM (solid).

and at $x_F \lesssim -0.3$ ($y^* \lesssim -2.5$) for pN collisions.

In Fig. 9(c) we display the ratio of normalized inclusive rapidity spectra,

$$R(y^*)=\frac{(\sigma_{in}^{-1}d\sigma/dy^*)_{p\,Ne}}{(\sigma_{in}^{-1}d\sigma/dy^*)_{pN}}\ , \tag{14}$$

for K_S^0 in p ^{20}Ne and pN interactions. For comparison, our data for γ conversions[12,27] are also plotted; at $y^* \lesssim -2.0$ the ratio $R(y^*)$ for K_S^0 mesons is slightly higher than that for γ's (which originate mostly from π^0 and η^0 decays).

The shapes of the $p_\perp^2$ spectra for K_S^0 mesons [Fig. 11(a)] are roughly similar for p ^{20}Ne and pN interactions, although the ratio

$$R(p_\perp^2)=\frac{(\sigma_{in}^{-1}d\sigma/dp_\perp^2)_{p\,Ne}}{(\sigma_{in}^{-1}d\sigma/dp_\perp^2)_{pN}} \tag{15}$$

dips slightly near $p_\perp^2 \sim 0.5$ [see Fig. 11(b)].

We note that, similar to other experiments (e.g., see Refs. 14–18, 36, and 38–40), we observe a "kink" in our $p_\perp^2$ spectra at $p_\perp^2 \simeq 0.3$–0.4 GeV/c both in p ^{20}Ne and pN data. Some authors explain this nonmonotonic behavior as a contribution of two independent mechanisms of strange-particle production.

B. Λ^0 hyperons

The y^*, x_F, and $p_\perp^2$ spectra of Λ^0 hyperons in p ^{20}Ne and pN interactions are shown in Figs. 12–14. For comparison, in Fig. 12(b) data for pp interactions at 303 GeV/c are shown.[14] We conclude that both experiments are in agreement. It is also interesting to note that, com-

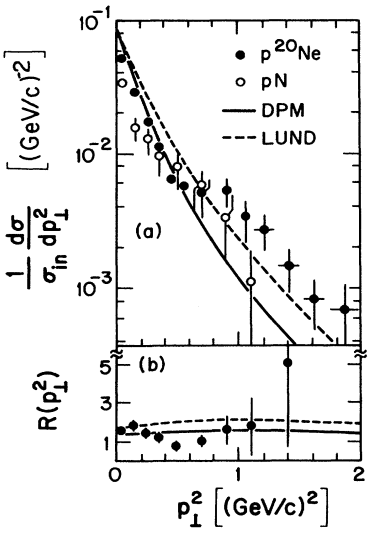

FIG. 11. (a) The $p_\perp^2$ distributions of K_S^0 mesons in p ^{20}Ne and pN interactions. (b) The ratio $R(p_\perp^2)$ for p ^{20}Ne and pN interactions [see Eq. (15) in the text]. The curves are the predictions of the LM (dashed) and the DPM (solid) for p ^{20}Ne interactions.

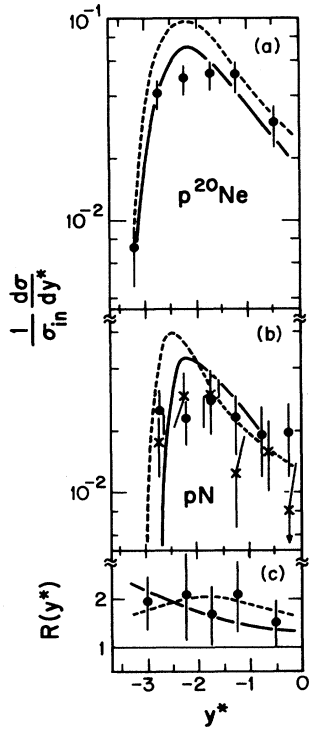

FIG. 12. The rapidity spectra for Λ^0 in the (a) p ^{20}Ne and (b) pN interactions. Also shown in (b) are data for pp interactions at 303 GeV/c (Ref. 14) (crosses). In (c) the ratio of normalized spectra $R(y^*)$ for Λ^0 in the p ^{20}Ne and pN interactions [see Eq. (16) in the text] is shown. The curves are predictions of the LM (dashed lines) and the DPM (solid lines).

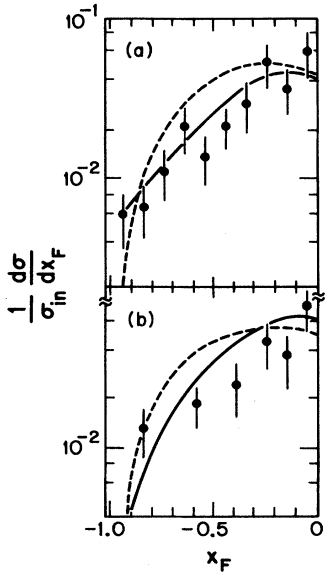

FIG. 13. The x_F spectra for Λ^0 in the (a) p ^{20}Ne and (b) pN interactions. The curves are predictions of the LM (dashed) and the DPM (solid).

pared to K_S^0 data, the ratio

$$R(y^*)=\frac{(\sigma_{in}^{-1}d\sigma/dy^*)_{p\,\mathrm{Ne}}}{(\sigma_{in}^{-1}d\sigma/dy^*)_{pN}} \tag{16}$$

for Λ^0 hyperons [Fig. 12(c)] has no apparent dependence on y^*, although, in this case, experimental errors are larger. We can also conclude from comparison of Λ^0

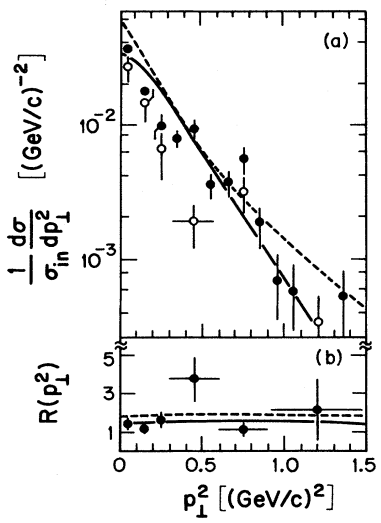

FIG. 14. (a) The $p_\perp^2$ distributions for Λ^0 hyperons in p ^{20}Ne and pN interactions. The curves are predictions of the LM (dashed) and the DPM (solid) for p ^{20}Ne interactions. In (c) the ratio of the normalized rapidity spectra $R(p_\perp^2)$ for the p ^{20}Ne and pN interactions is shown for Λ^0. The dashed line is the LM prediction and the solid line is the DPM prediction.

spectra with our versions of the Lund model and the dual parton model that the latter is in better agreement with data for both p ^{20}Ne and pN interactions.

IX. Λ^0 POLARIZATION

Because of parity conservation in the strong interaction, Λ^0 can only be polarized in the direction transverse to the production plane, i.e., relative to the normal

$$\hat{\mathbf{n}}=\frac{\mathbf{p}_0\times\mathbf{p}_\Lambda}{|\mathbf{p}_0\times\mathbf{p}_\Lambda|}\ , \tag{17}$$

where $\mathbf{p}_0$ and $\mathbf{p}_\Lambda$ are the momentum vectors of the primary particle and Λ^0 hyperon, respectively.

Then the Λ^0 polarization p_Λ is determined from the expression

$$p_\Lambda=\frac{3\langle\cos\theta^*\rangle}{\alpha_\Lambda}\ , \tag{18}$$

where $\alpha_\Lambda=0.642\pm0.013$ is the asymmetry parameter[37] of Λ^0 decay and θ^* is the angle between the momentum vector of the proton in the rest system of Λ^0 and the unit vector $\hat{\mathbf{n}}$ from Eq. (17).

From the analysis of our data we find

$$p_\Lambda(p\ ^{20}\mathrm{Ne})=-(0.12\pm0.06)$$
$$\text{in } p\ ^{20}\text{Ne interactions} \tag{19}$$

and

$$p_\Lambda(pN)=-(0.01\pm0.11)\ \text{ in } pN \text{ events}\ . \tag{20}$$

As shown in Fig. 15, the result for $p_\Lambda(pN)$ is in agreement with data from π^-p and pp interactions.[39,41,42,9]

In Fig. 16 we display p_Λ as a function of the transverse momentum of Λ^0. Our data for Λ^0 with $x_F\leq0$ are in agreement with measurements of Λ^0 polarization in the very forward ($x_F\gg0$) direction,[39,41,42,9] which indicate a

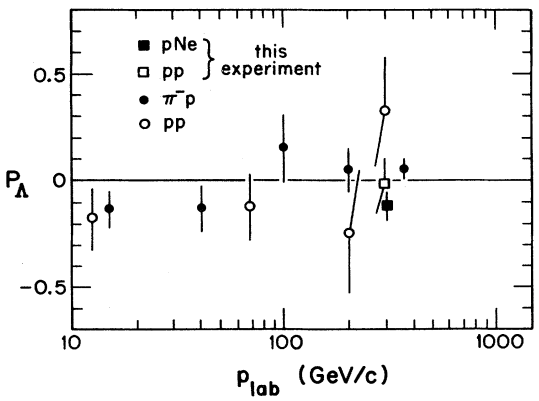

FIG. 15. The polarization of Λ^0 hyperons as a function of the momentum of the incident proton.

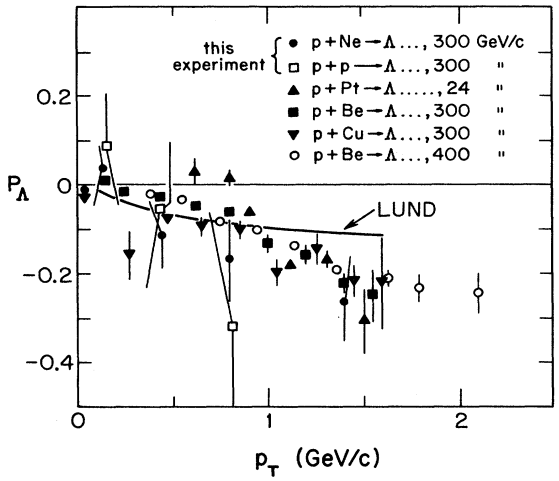

FIG. 16. The $p_\perp$ dependence of Λ^0 polarization (data from Refs. 39, 41, 42, and 9). Data from this experiment with $x_F \leq 0$ agrees with data from the forward region $x_F >> 0$. The solid line shows the predictions of the Lund model (Ref. 1) for the pp interactions.

decrease of p_Λ with $p_\perp$. The solid line in Fig. 16 represents a calculation of p_Λ using the Lund model; the polarization of Λ^0 hyperons occurs as a result of the compensation of the angular momentum of sea $(s\bar{s})$ pairs by spins of $s(\bar{s})$ quarks. The data are in qualitative agreement with theoretical expectations.

We emphasize, however, that the Λ^0 polarization measured in this experiment is not a measurement of p_Λ for "direct" Λ^0 because, as shown in Sec. VII, more than 40% of the observed Λ^0 come from $\Sigma^0 \rightarrow \Lambda^0\gamma$ decay, for which $p_\Lambda = -p_\Sigma/3$. Other measurements[39,41] and theory[43] indicate that the polarization of "direct" Λ^0 can be larger than the experimentally measured value of p_Λ. For example, if the Σ^0 were unpolarized then the polarization of direct Λ^0 would be increased in magnitude 1.75. If the polarization $p_\Sigma = p_\Lambda$, the polarization would increase in magnitude by 2.3.

X. CONCLUSION

In this paper we have presented experimental data on inclusive production of K_S^0 mesons and Λ^0 hyperons at $x_F \leq 0$ in p ^{20}Ne and pN interactions at 300 GeV/c. We find the average multiplicity of K_S^0 and Λ^0 produced on neon is higher (approximately 1.5 and 2.0 times, respectively) than from a nucleon target. We observe strong correlations between the mean multiplicity, $\langle n(V^0)\rangle$, of V^0 particles and the number of charged pions. In addition, for p ^{20}Ne interactions, we observe such correlations between $\langle n(V^0)\rangle$ and the multiplicity of secondary protons (fragments of a nucleus). Using model calculations to estimate and subtract effects due to Fermi motion, we estimate the production cross sections and mean multiplicity due to cumulative V^0 particles.

Approximately 43% of observed Λ^0 are produced via $\Sigma^0 \rightarrow \Lambda^0\gamma$ decays. We also observe production of $K^{*0}(892)$ and $K^{*0}(1415)$ meson resonances and $\Sigma^0(1385)$ and $\Sigma(1670)$ strange isobars.

The inclusive spectra for V^0 particles are presented, as are polarization measurements for the Λ^0.

These data are compared with Monte Carlo calculations produced in the framework of the Lund model[1] (version FRITIOF-2) and the dual parton model[3] proposed for soft hadron-nucleus and hadron-nucleon interactions. In general, both models provide reasonable qualitative agreement for neutral-strange-particle production in p ^{20}Ne and pN interactions. However, the Lund model tends to overestimate the absolute yields of K^0 and Λ^0.

ACKNOWLEDGMENTS

We wish to express our sincere appreciation to the scanning and measuring staffs at Tashkent and Wisconsin for their efforts and we acknowledge the fine efforts on the part of the 30-in. bubble-chamber crew at Fermilab. We gratefully acknowledge the efforts of Professor A. Erwin and other members of the Wisconsin group before and during the data-taking phase of the experiment. Our thanks go also to L. Voyvodic for help and encouragement. One of us (B.S.Y.) thanks Professor H. J. Lubatti for fruitful discussions and hospitality during a stay at the University of Washington.

*Present address: Institute of Nuclear Physics, The Uzbek Academy of Sciences, Ulugbek, Tashkent 702132, U.S.S.R.

[1] B. Andersson, G. Gustafsson, and B. Nilsson-Almqvist, Nucl. Phys. **B281**, 289 (1987).
[2] B. Nilsson-Almqvist and E. Stenlund, Comput. Phys. Commun. **43**, 387 (1987).
[3] A. M. Zadorozhni, Sh. Yu. Shmakov, V. V. Uzhinksii, Yad. Fiz. **39**, 1155 (1984) [Sov. J. Nucl. Phys. **39**, 729 (1984)]; A. Polanski, S. Yu. Shmakov, and V. V. Uzhinskii, Joint Institute for Nuclear Research Reports Nos. E2-88-732, 1988 (unpublished), E2-88-793, 1988 (unpublished), and P2-86-381, 1986 (unpublished).
[4] N. K. Glendenning and J. Rafelski, Phys. Rev. C **31**, 823 (1985).
[5] J. Kapusta and A. Mekjian, Phys. Rev. D **33**, 1304 (1986).
[6] P. Koch *et al.*, Z. Phys. C **38**, 269 (1988).
[7] P. Koch *et al.*, Mod. Phys. Lett. A **3**, 737 (1988).
[8] P. Koch *et al.*, Phys. Rep. C **142**, 167 (1986).
[9] L. G. Pondrom, Phys. Rep. **122**, 57 (1985).
[10] Kam-Biu Luk, Report No. Fermilab-Conf-89/40, 1989 (unpublished).
[11] S. A. Azimov *et al.*, Yad. Fiz. **33**, 169 (1981) [Sov. J. Nucl. Phys. **33**, 87 (1981)].
[12] Kh. Kh. Artykov *et al.*, Yad. Fiz. **43**, 1472 (1986) [Sov. J. Nucl. Phys. **43**, 949 (1986)].
[13] S. A. Azimov *et al.*, Phys. Rev. D **23**, 2512 (1981).
[14] A. Sheng *et al.*, Phys. Rev. D **11**, 1733 (1980).
[15] F. LoPinto *et al.*, Phys. Rev. D **22**, 573 (1980).
[16] M. Asai *et al.*, Z. Phys. C **27**, 11 (1985).
[17] R. D. Kass *et al.*, Phys. Rev. D **20**, 605 (1979).

[18]G. Charlton *et al.*, Phys. Rev. Lett. **29**, 1759 (1972).
[19]G. Charlton *et al.*, Phys. Rev. Lett. **30**, 574 (1973).
[20]K. Heller *et al.*, Phys. Rev. D **16**, 2737 (1977).
[21]S. P. Denisov *et al.*, Nucl. Phys. **B61**, 62 (1973).
[22]D. Antreasyan *et al.*, Phys. Rev. D **19**, 764 (1979).
[23]V. V. Abramov *et al.*, Z. Phys. C **24**, 205 (1985).
[24]V. V. Abramov *et al.*, Yad. Fiz. **41**, 357 (1985) [Sov. J. Nucl. Phys. **41**, 227 (1985)].
[25]U. Becker *et al.*, Phys. Rev. Lett. **37**, 1731 (1976).
[26]P. Skubic *et al.*, Phys. Rev. D **18**, 3115 (1978).
[27]B. S. Yuldashev *et al.*, following paper, Phys. Rev. D **43**, 2803 (1991).
[28]S. A. Azimov *et al.*, Yad. Fiz. **33**, 1562 (1981) [Sov. J. Nucl. Phys. **33**, 841 (1981).
[29]B. Andersson *et al.*, Phys. Lett. **73B**, 343 (1978).
[30]W. Busza, Acta. Phys. Pol. B **8**, 119 (1977).
[31]N. N. Nikolaev, Usp. Fiz. Nauk **134**, 369 (1981) [Sov. Phys. Usp. **24**, 531 (1981)].
[32]S. A. Azimov *et al.*, Czech. J. Phys. B **35**, 920 (1985).
[33]M. L. Allaberdin *et al.*, Yad. Fiz. **39**, 662 (1984) [Sov. J. Nucl. Phys. **39**, 420 (1984)].
[34]B. S. Yuldashev *et al.*, Wisconsin Report No. WISC-EX-90-310, 1990 (unpublished).
[35]R. Singer *et al.*, Nucl. Phys. **B135**, 265 (1978).
[36]H. Kichimi *et al.*, Phys. Rev. D **20**, 37 (1979).
[37]Particle Data Group, M. Aguilar-Benitez *et al.*, Phys. Lett. B **204**, 1 (1988).
[38]H. Kichimi *et al.*, Lett. Nuovo Cimento **24**, 129 (1979).
[39]E. N. Kladnitzkaya, Elem. Part. Nuclei **13**, 669 (1982).
[40]M. Asai *et al.*, Institut für Hochenenergiephysik Report No. 85-65, 1985 (unpublished).
[41]T. Haupt, Institute of Nuclear Physics Report No. 1292/pH, 1985 (unpublished).
[42]K. Heller *et al.*, Phys. Rev. Lett. **51**, 2025 (1983); L. Schachinger *et al.*, *ibid.* **52**, 581 (1984).
[43]R. Gattio, Phys. Rev. **109**, 610 (1958).